Efficient time-domain numerical analysis of waveguides with tailored wideband pulses

Jonathan Viquerat

HAL Id: hal-02433052
https://hal.inria.fr/hal-02433052

Efficient time-domain numerical analysis of waveguides with tailored wideband pulses

Jonathan Viquerat

Abstract—**A simple procedure for the generation of accurate polychromatic sources in waveguides taking into account mode dispersion is presented. It allows for an efficient use of time-domain solvers in the analysis of guided modes, and can be used wether the mode dispersion and field distribution are known analytically or numerically. This method is implemented in the DIOGENES Discontinuous Galerkin Time-Domain (DGTD) solver (http://diogenes.inria.fr), and is validated on a waveguide mode converter.**

Index Terms—**Discontinuous Galerkin Time-Domain (DGTD) methods, optical waveguides, mode dispersion, wide-band source.**

I. INTRODUCTION

THE numerical analysis of optical devices with time-domain methods usually allows the use of polychromatic sources (dipole, plane wave, etc), thus characterizing the structure response in a single simulation. For waveguides, however, the existence of modes brings the task of building wide-band sources to a higher level of complexity [1]. More precisely, two main obstacles must be overcome: (i) for a given mode, the effective index n_{eff} depends on ω, and (ii) the frequency-domain 2D mode field distribution $\hat{\mathbf{E}}_{\text{2D}}$ also depends on ω.

The bootstrapping method, proposed in [1], is an effective yet computationally-expensive way to overcome these problems. An erroneous source is injected and propagated in an extended version of the considered waveguide. Along the propagation, the exact mode establishes in the waveguide, while the remaining energy is scattered towards the surrounding PML regions. At the edge of the waveguide, a probe plane is used to record passing fields, providing an accurate source for future computations.

In [2], the authors propose another workaround, in which a wide-band source made from the sum of several polychromatic pulses. Each of them is centered around a given frequency and holds an appropriate 2D field distribution associated to this frequency. In this method, the sampling of the 2D field distribution and that of the effective mode index are concurrently made at the selected frequencies, which are most often limited to a handful.

In this paper, we propose a straightforward polychromatic source formulation for waveguide analysis based on an inverse Fourier transform of the frequency-domain solution, incorporating both the variations of the 2D field distribution and that of the mode index. The knowledge of both these quantities can

J. Viquerat is with the INRIA Sophia-Antipolis research center, 06902 France. E-mail: jonathan.viquerat@inria.fr.

be either analytic or numeric (*i.e.* computed in a third-party solver or read from a file). Additionally, we describe the way to impose of such a source through a Total-Field/Scattered-Field (TF/SF) interface in the DGTD framework, as well as how to compute figures of merit such as transmission, overlap or mode conversion efficiency. The accuracy of this approach is first tested on a textbook case, before being applied to a waveguide mode converter.

II. DESCRIPTION OF THE SOURCE

A. Source construction

Assuming that $\hat{\mathbf{E}}_{\text{2D}}$ and n_{eff} are known, we remind that the corresponding monochromatic time-domain source propagating in direction $\mathbf{z}_+$ at angular frequency ω_0 is obtained as follows:

$$\mathbf{E}(t) = \Re\left[\hat{\mathbf{E}}_{\text{2D}}(\omega_0)\mathrm{e}^{-j\beta(\omega_0)z}\mathrm{e}^{j\omega_0 t}\right],$$

where $\beta(\omega)$ is the mode propagation constant:

$$\beta(\omega) = \frac{\omega n_{\text{eff}}(\omega)}{c_0}. \tag{1}$$

For plane wave analysis, polychromatic signals are most often obtained by modulating a sine or a cosine function at angular frequency ω_0 with the derivative of a gaussian bump centered on ω_0 and with well-suited variance parameter σ. Then, taking the Inverse Fourier Transform (IFT) of the frequency-domain signal yields the desired time-domain pulse. One can follow the same procedure here, taking into account the effective index of the mode:

$$\mathbf{E}(t) = \Re\left[\int_{-\infty}^{+\infty} \hat{\mathbf{E}}_{\text{2D}}(\omega)\sigma\mathrm{e}^{-\frac{(\omega-\omega_0)^2\sigma^2}{2}}\mathrm{e}^{-j(\beta(\omega)z-\omega t)}\right] \tag{2}$$

Most often, the latter IFT is not analytic and must be numerically computed using an Inverse Discrete Fourier Transform (IDFT):

$$\phi(t) \simeq \sum_{k=1}^{n_\omega} \hat{\phi}(\omega_k)\mathrm{e}^{j\omega_k t}\Delta\omega, \tag{3}$$

where $\Delta\omega$ is the chosen frequency step:

$$\omega_k = \omega_{\text{min}} + (k-1)\Delta\omega,$$

and n_ω is the number of frequency samples:

$$n_\omega = \frac{\omega_{\text{max}} - \omega_{\text{min}}}{\Delta\omega} + 1.$$

B. Sampling and the reciprocal Shannon theorem

The choice of n_ω (or equivalently of $\Delta\omega$) will have a major impact on the accuracy and efficiency of the procedure. Indeed, if it is chosen too high, the frequency-domain expression under the integral in (3) will be over-sampled, and its evaluation will be uselessly expensive. On the opposite, if it is chosen too low, the obtained time-domain signal will suffer from aliasing, resulting in overlapping incident wave trains. In order to select an adequate value for n_ω, we make use of the reciprocal Shannon theorem [3], stating that the sampling rate $\Delta\omega$ used to compute (3) should meet the following criterion:

$$\Delta\omega \leq \frac{2\pi}{T},$$

where T is the total duration of the transformed time-domain signal. Although in most cases, T might not be known, in our case it can be well approximated thanks to the Gaussian envelope of the frequency-domain expression (2). To do so, we introduce a parameter ϵ, such that fields with amplitudes smaller than ϵ are considered to be zero. Then, we seek the width of the gaussian enveloppe for which the signal level is equal to ϵ. A few lines of calculus yield:

$$\Delta\omega = \frac{2\pi}{\sigma\sqrt{8\ln(\frac{1}{\epsilon})}}. \tag{4}$$

In the following, we choose $\epsilon = 1 \times 10^{-3}$, and therefore:

$$\Delta\omega \simeq \frac{0.845}{\sigma}. \tag{5}$$

C. Total-Field/Scattered-Field injection plane

The discretization of the electric and magnetic fields in the DGTD framework is naturally discontinuous, meaning that the unknowns are duplicated on each face joining two cells of the mesh [4]. The consistency of the approximation is re-established through the imposition of a *numerical flux* $(\mathbf{E}_*, \mathbf{H}_*)$ at the interface, which handles the information exchange between cells (the reader is referred to [4] and [5] for a thorough development of the DGTD method). As a consequence, it is possible to define separate areas in the mesh, in which the numerical unknowns either hold the total fields $(\mathbf{E}_{tot}, \mathbf{H}_{tot})$ or the scattered fields $(\mathbf{E}_{sca}, \mathbf{H}_{sca})$. The interface between these regions is the so-called TF/SF interface. At this interface, the fluxes are modified in order to inject the incident field in the TF region, and to subtract it in the SF region (see figure 1). With this method:

- It is possible to access both the TF and the SF fields in their regions of interest simultaneously;
- Incident fields can be imposed virtually anywhere in the mesh;
- Accessing both the TF and SF fields at the same place (*i.e.* on the TF/SF interface) allows for the computation of multiple figures of merit with a single computation;
- In the present case, if a mode is properly imposed and propagated through the TF region of an unperturbed waveguide, the fields in the SF regions should be identically zero, making it a reliable method to test the source described in the last section.
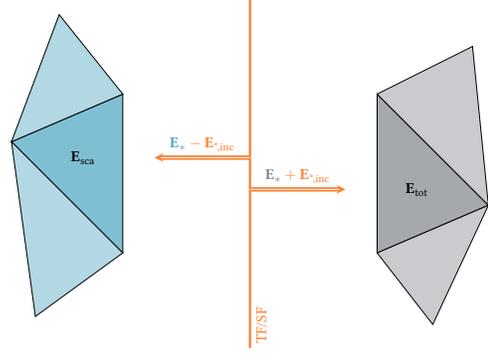
Fig. 1. **Field injection with the TF/SF method.** In the TF zone (in gray), the incident field is added to the numerical flux, whereas in the SF zone, it is substracted.

D. Figures of merit

A brief word must be said about the figures of merit that will be used in this paper, namely the transmission T, the overlap O_M and the mode conversion efficiency η_M.. These quantities are based on the computation of the averaged Poynting vector $\boldsymbol{\pi}$:

$$\boldsymbol{\pi}(\mathbf{x},\omega) = \frac{1}{2}\Re\left(\widehat{\mathbf{E}}(\mathbf{x},\omega) \times \widehat{\mathbf{H}}^*(\mathbf{x},\omega)\right). \tag{6}$$

In expression (6), the frequency-domain fields are evaluated on control surfaces (here, the TF/SF surfaces) with an on-the-fly Fourier transform during the time-domain computation. Thanks to the discontinuous nature of the DG field discretization, these quantities can be evaluated either on the total-field or the scattered-field side of the TF/SF faces, allowing to compute the transmission as:

$$T(\omega) = \frac{\displaystyle\int_{S_o} \boldsymbol{\pi}_{tot} \cdot \mathbf{n}}{\displaystyle\int_{S_i} \boldsymbol{\pi}_{inc} \cdot \mathbf{n}}, \tag{7}$$

where $\boldsymbol{\pi}_{tot}$ is computed on the total-field side of the exiting TF/SF surface S_o, $\boldsymbol{\pi}_{inc}$ is computed using the incident field only on the total-field side of the inputting TF/SF surface S_i, and $\mathbf{n}$ is the unit normal. As such, the transmission computes the normalized transmitted power from the input to the output plane, ranging from 0 to 1. The overlap, also ranging from 0 to 1, measures the similarity of the transmitted fields $\widehat{\mathbf{E}}$ and $\widehat{\mathbf{H}}^*$ to that of a given mode $\widehat{\mathbf{E}}_M$ and $\widehat{\mathbf{H}}_M^*$:

$$O_M(\omega) = \frac{\Re\left(\dfrac{\Pi_{S_o}\left(\widehat{\mathbf{E}}, \widehat{\mathbf{H}}_M^*\right)\Pi_{S_o}\left(\widehat{\mathbf{E}}_M, \widehat{\mathbf{H}}^*\right)}{\Pi_{S_o}\left(\widehat{\mathbf{E}}, \widehat{\mathbf{H}}^*\right)}\right)}{\Re\left(\Pi_{S_i}\left(\widehat{\mathbf{E}}_M, \widehat{\mathbf{H}}_M^*\right)\right)}, \tag{8}$$

with:

$$\Pi_S\left(\widehat{\mathbf{E}}, \widehat{\mathbf{H}}^*\right) = \int_S \widehat{\mathbf{E}} \times \widehat{\mathbf{H}}^* \cdot \mathbf{n}.$$
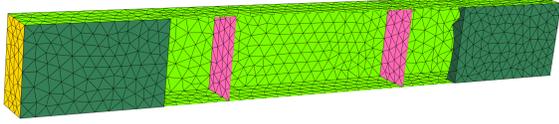
Fig. 2. **Mesh of the rectangular waveguide.** Light green faces correspond to PEC boundaries, while yellow ones are for ABC. The pink inner faces correspond to the TF/SF interfaces. The TF cells (not shown) are between the two TF/SF interfaces, while the SF cells (not shown) are on the left and the right of them. The PML cells terminate the mesh on the edges (in dark green).

Finally, the mode conversion efficiency, which computes the normalized transmitted power that has been coupled to a given mode M, is easily defined as:

$$\eta_M(\omega) = T(\omega)O_M(\omega).$$

III. NUMERICAL EXPERIMENTS

A. Straight rectangular waveguide

We consider a rectangular waveguide of lateral dimensions $a = 10.16$ mm and $b = 22.86$ mm with PEC (Perfect Electric Conductor) walls. The goal of this section is to propagate a TE_{01} mode in it, and to assess the efficiency and accuracy of the procedure described above. The operating frequency range is $[8, 10]$ GHz. We exploit a high-order DGTD method [5] on an adequately-refined tetrahedral mesh. The incident field is imposed on a Total-Field/Scattered-Field interface, separating a total field region (in the center of the numerical domain) from a scattered field region (before the input and after the output). The mesh, shown in figure 2, is terminated on both ends with a Perfectly-Matched Layer (PML) region to absorb outgoing field.

As a first experiment, we consider the propagation of an uncorrected polychromatic pulse, where frequency dependence of $\hat{\mathbf{E}}_{2D}$ and β is *not* taken into account. Both the quantities are approximated by their evaluation at the central frequency $f_c = 9$ GHz. To evaluate the quality of the numerical treatment, we simply consider the evaluation of the E_y component of the electric field at a chosen probe point in the SF region. Thanks to the use of TF/SF interfaces, for an unperturbed waveguide the field should be identically equal to 0 in the SF regions. In figure 3, we show a 3D snapshot of the field during computation: the presence of field in the right SF region indicates a mismatch between the numerical solution and the expected exact solution. Such a result was to be expected, since most frequencies in the pulse were numerically transported with an erroneous propagation constant.

We now consider the ω dependence of the quantities involved. The effective index of the mode is plotted in figure 4, along with the resulting spectral power of the incident pulse.

In figure 5, we conduct the same experiment as before, but using expression (2) for the omega-dependent quantities. Using expression (4) gives $n_\omega = 24$ for this computation. A 3D snapshot of the computed electric field is shown in figure 5. For a better comparison, we plot in figure 6 a comparative time-domain plot of E_y in the right SF region,
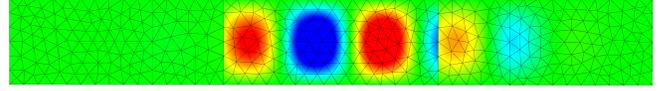
Fig. 3. **Snapshot of the E_y field during computation for an uncorrected polychromatic pulse.** The presence of field in the right SF region indicates a mismatch between the numerical solution and the expected exact solution. The field discontinuity at the interface between TF and SF regions is a natural consequence of the TF/SF injection method. Field values are scaled in the range $[-1, 1]$ V/m.
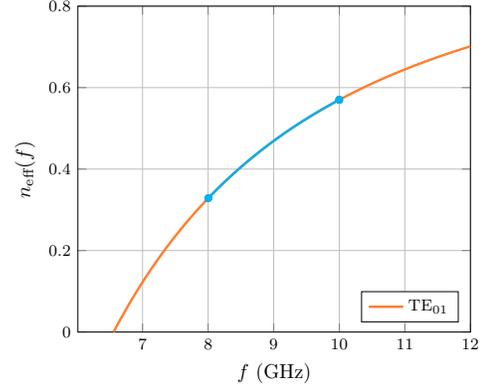
(a) TE_{01} mode effective index and selected frequency range
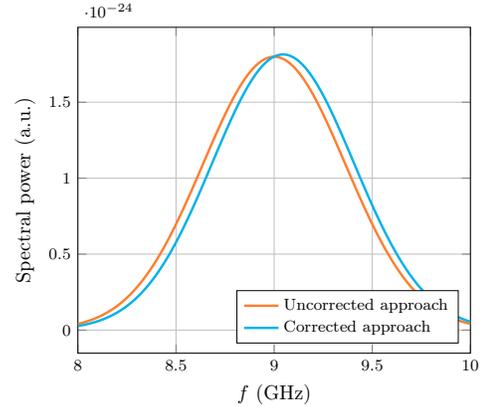
(b) Spectral power (arbitrary units) of the incident pulse in the regular and corrected cases

Fig. 4. **TE_{01} mode index spectral power of the incident pulse** in the uncorrected and corrected approaches.

with and without the IDFT correction. As can be seen, taking into account the ω dependance of the incident field and index greatly improves the mode mismatch. The maximal L^2 errors on the electric field observed in the right SF region, with and without mode correction, are shown in table I, along with the corresponding CPU times. The computed error is 60 times lower with the mode correction, while the CPU times is increased by 34%, thus confirming the interest of this method.

B. TE_{01}-TE_{02} mode converter

We now consider a TE mode converter, as presented in [6]. The converter is composed of a bent rectangular PEC waveguide of dimensions $a = 22.15$ mm and $b = 47.55$ mm. The bending is tailored for a theoretical power conversion of
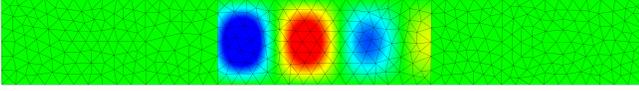
Fig. 5. **Snapshot of the E_y field during computation with a corrected polychromatic pulse.** The absence of field in the right SF region indicates that the transported numerical solution and the expected exact solution match. Field values are scaled in the range $[-1, 1]$ V/m.
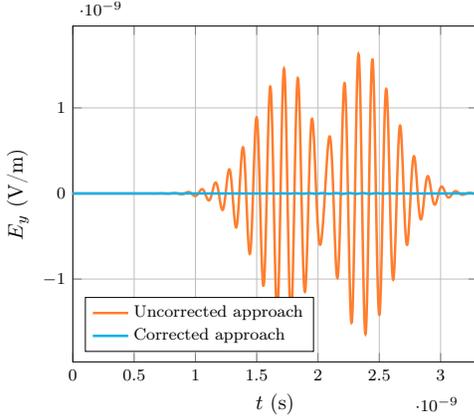
Fig. 6. **Time-domain plots of the E_y field in the right SF region with a corrected and an uncorrected pulse.** We observe a very small residual error with the corrected approach, due to the inaccuracies in the Inverse Discrete Fourier Transform (IDFT).

Fig. 7. **TE_{01}, TE_{02} and TE_{10} modes effective indices.** The selected frequency range is indicated in light blue.

Fig. 8. **Computed mode conversion efficiency from TE_{01} to TE_{02} in the selected frequency range** with the uncorrected and the corrected pulses. As expected, the same conversion efficiency is observed for $f = 8.5$ GHz. The mode mismatch at the lowest frequency induces a 2.5% discrepancy in the computed conversion rate.

100% at $f = 8.5$ GHz. The goal of this section is to assess the converter efficiency in the $[7.5, 8.5]$ GHz frequency range in a single run, using the technique presented above. The effective indices of the two modes in the selected frequency range are shown in figure 7. As it shall be useful later, we also plot in the latter figure the effective index of the TE_{10}, which is the only other mode which effective index is real in the frequency range of interest. Following the results of the previous section, n_ω is set to 24 for this experiment. The mode conversion efficiency from TE_{01} to TE_{02} is computed following the details of section II-D, and is shown in figure 8 for both pulses. As expected, a peak efficiency of 1 is found for $f = 8.5$ GHz in both cases, while it decays for lower frequencies. However, the uncorrected approach overestimates the conversion rate from roughly 2.5 % at the minimal frequency. The obtained results are in line with what was found in [6]. Similarly to the previous section, the CPU time is increased by roughly 30.5% when using the mode-corrected source.

Snapshots illustrating the mode conversion are shown in figure 9. The TE_{01} mode pulse is incoming from the left, before being converted in a TE_{02} that leaves the computational

domain from the right (full mesh is not shown here). To complete the study, we compute the conversion efficiencies $\eta_{TE_{01}}$ and $\eta_{TE_{10}}$, *i.e.* the normalized amount of energy coupled from the TE_{01} mode at the input to the TE_{01} and TE_{10} modes at the output. Results, presented in figure 10, show that for lower frequencies, a non-negligible part of the pulse is not converted to the TE_{02} mode. On the other hand, the conversion rate to TE_{10} mode is identically 0. It should be noted that a very low level of backscattering was observed in the computations, hence it is not plotted here.

IV. CONCLUSION

In this paper, we provided a simple expression for the computation of accurate polychromatic sources in waveguides. Details about its practical use were also discussed, such as the minimal frequency-domain sampling or the use of TF/SF faces to impose it in the computational domain. The computation of relevant figures of merit was also sketched. The described procedure was then validated on a microwave-regime rectangular waveguide, on which significantly low error levels were observed. Finally, the method was applied to a real-life mode converter, allowing to assess the device response on a large bandwidth in a single computation.

TABLE I
MAXIMAL L^2 ERRORS AND CPU TIMES WITH AND WITHOUT MODE CORRECTION.

	Non-corrected	Corrected
CPU time (s.)	101	135
Max. error	1.71×10^{-1}	2.83×10^{-3}
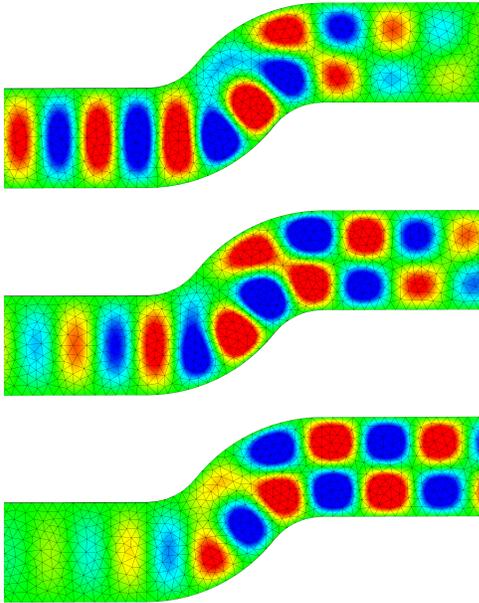
Fig. 9. **Successive E_x field snapshots during the conversion of a polychromatic TE_{01} mode to a TE_{02} mode.** Full mesh is not shown here.
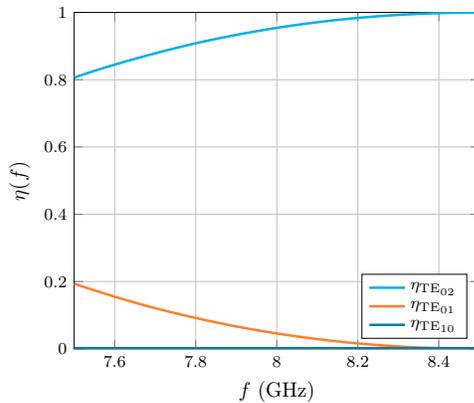
Fig. 10. **Computed mode conversion efficiency from TE_{01} at the input to TE_{01}, TE_{02} and TE_{10} modes at the output.**

REFERENCES

[1] A. Taflove and S. Hagness, *Computational Electrodynamics: The Finite-Difference Time- Domain Method*, 3rd ed. Artech House, Boston, 2005.

[2] J. Yamauchi, S. Sasaki, and H. Nakano, "Pulse excitation scheme for the analysis of wide-band characteristics of optical waveguides," *IEEE Photonics Technology Letters*, vol. 17, pp. 357 – 359, 2005.

[3] G. S. Khanyan, "Sampling theorem in frequency domain for the infinite spectrum," in *IEEE East-West Design & Test Symposium (EWDTS)*, 2017.

[4] J. S. Hesthaven and T. Warburton, *Nodal discontinuous Galerkin methods*. Springer, 2008.

[5] J. Viquerat, "Simulation of electromagnetic waves propagation in nano-optics with a high-order discontinuous Galerkin time-domain method," Ph.D. dissertation, INRIA Sophia-Antipolis, 2015.

[6] Q. Zhang, C. W. Yuan, and L. Liu, "Theoretical design and analysis for TE20-TE10 rectangular waveguide mode converters," *IEEE Transactions on Microwave Theory and Techniques*, vol. 60, pp. 1018 – 1026, 2012.